Available online at www.sciencedirect.com
ScienceDirect
Catalysis Today 130 (2008) 97–108
CATALYSIS TODAY
www.elsevier.com/locate/cattod

Aging of Co(Ni)MoP/Al_2O_3 catalysts in working state

B. Guichard [a], M. Roy-Auberger [a], E. Devers [a,*], C. Legens [b], P. Raybaud [c]

[a] *IFP-Lyon, Direction Catalyse et Séparation, BP No. 3, 69390 Vernaison, France*
[b] *IFP-Lyon, Direction Physique et Analyse, BP No. 3, 69390 Vernaison, France*
[c] *IFP, Direction Chimie et Physico-chimie Appliquées, 1 et 4 Avenue Bois Préau, 92500 Rueil-Malmaison, France*

Abstract

The deactivation behavior of Co(Ni)MoP/Al_2O_3 catalysts during diesel fuel hydrotreatment is investigated by means of X-ray photoelectron spectroscopy (XPS) and transmission electron microscopy (TEM). XPS measurements performed on aged Co(Ni)MoP/Al_2O_3 catalysts show that the promoter quantity on the edges of MoS_2 nano-crystallites decreases with increasing lifetime. TEM coupled with energy dispersive X-ray spectrometry (EDX) indicates that the Co(Ni)/Mo ratio inside crystallites changes without any modification over MoS_2 layers (size and stacking). Moreover toluene hydrogenation activity loss on aged catalysts is found to be linearly correlated to the XPS promotion rate decrease during deactivation.

These experimental results have been analyzed in the light of recent density functional theory (DFT) calculations on the thermodynamic stability of Co(Ni)MoS phases in sulfo-reductive working conditions. It is shown that the destabilization of the mixed phase may be partially attributed to the reaction conditions (high temperature and reductive environment). In addition, the role of the coke cannot be excluded to explain the promotion rate decrease revealed by XPS spectra. The experimental results combined with DFT results are used to propose an origin of the active phase modifications in working state.

Keywords: NiMoS; CoMoS; Active mixed phase; DFT; XPS; TEM; Deactivation; Segregation

1. Introduction

Owing to the strengthening of the environmental legislation, production of ultra-low sulfur diesel fuels remains an essential issue for refiners. Catalysts used for hydrotreating are generally composed of sulfided molybdenum promoted by nickel or cobalt and supported on alumina. As proposed by the geometrical model of Kasztelan et al. [1], the active phase consists of particles closed to hexagonal MoS_2 nano-crystallites decorated by Co and Ni promoters and it is now well established that the active sites for HDS are located on the edges of the crystallites [2]. By 2009, the sulfur specification in diesel fuels will be decreased to 10 ppm. This level can be reached by hardening the working conditions (increase of temperatures, for example) or by using more active catalysts. In both cases, crucial questions about the stability of the catalyst and its active phase are raised. The deactivation of hydrotreating catalysts has been the subject of numerous studies. Two main causes are generally invoked in the literature. The first one is the accumulation of coke inside the pores of the catalyst which prevents reactive molecules from accessing the active sites. Most authors have shown that coke becomes more aromatic with processing time-on-stream [3–6] and goes to a graphite-like structure. The second cause of deactivation may be the modification of the active phase itself resulting to particles sintering [7] or segregation of the promoter which was initially in decoration of MoS_2 slabs. Promoter segregation from the mixed phase has been quoted in the literature [8–11] even if not clearly elucidated. Recent progress in ab initio molecular modeling of sulfide catalysts [12–15] has made possible the investigation of the thermodynamic stability of the promoter at the edges of the Co(Ni)MoS nano-crystallites.

The crucial question of the promoter segregation and loss of the mixed active phase in working conditions is particularly addressed in this paper by performing XPS and TEM–EDX characterization on selected spent and fresh catalysts. The same series of catalysts will be also characterized by means of activity tests (toluene hydrogenation). The interpretation of the

* Corresponding author. Tel.: +33 4 78 02 27 63; fax: +33 4 78 02 20 66.
E-mail address: elodie.devers@ifp.fr (E. Devers).

0920-5861/$ – see front matter © 2007 Elsevier B.V. All rights reserved.
doi:10.1016/j.cattod.2007.09.007

Table 1
Origin of different aged NiMoP/Al_2O_3 catalysts

Origin	Feedstocks	Processing time (days)	Catalyst	T (K)	$p(H_2S)/p(H_2)$	$\Delta\mu_S$[a]
Fresh	–	0	Ni-0	–	–	–
Industrial plant	GO	730	Ni-A	620–650	~0.01	−1.00
	GO	365	Ni-B	620–650	~0.01	−1.00
	GO	730	Ni-C	620–650	~0.01	−1.00
	GO	730	Ni-D	620–650	~0.01	−1.00
Pilot plant	SRGO	47	Ni-E	613–623	0.013	−0.95
	GO coker	36	Ni-F	608–623	0.004	−1.01
	VGO	31	Ni-G	648–668	0.017	−0.96

[a] $\Delta\mu_S$ is the chemical potential of sulfur (expressed in eV) and is used in Fig. 6 (the reader could refer to [12,13,15,16] for a detailed explanation of this thermodynamic variable representing the working conditions T and $p(H_2S)/p(H_2)$).

observed experimental results will be proposed in the light of recent density functional theory (DFT) calculations on Co(Ni)MoS active phases [12–15]. Based on the DFT results reported in the present issue by Krebs et al. [12], we discuss the possible deactivation scheme occurring during the catalyst's life as a function of reaction conditions. We focus on the nickel and cobalt stability on the M-edge and S-edge of Co(Ni)MoS crystallites. The role of coke precursor adsorption on the edges will also be envisaged.

2. Experimental

2.1. Catalysts samples

2.1.1. Spent catalysts

Several spent Co(Ni)MoP/Al_2O_3 catalysts from two different origins were selected for this work. The first series (Ni-A to Ni-D and Co-A to Co-C) originates from industrial plants (IP) at the end of their lifetime. The second series (Ni-E to Ni-G and Co-D to Co-F) comes from pilot plants (PP) and corresponds to an intermediate state of deactivation. All spent catalysts come from the same generation of fresh Co(Ni)MoP catalysts. They are presented in Tables 1 and 2. Before characterization and activity measurements in toluene hydrogenation, spent catalysts were washed with a toluene reflux at 523 K and dried at 5 kPa and 423 K.

2.1.2. Fresh catalysts

The oxide precursors of Ni-0 and Co-0 commercial catalysts were prepared by impregnating a solution containing $(NH_4)_6[Mo_7O_{24}].4H_2O$, $(NO_3)_2Ni.6H_2O$ (or $(NO_3)_2Co.6H_2O$), H_3PO_4 and H_2O_2 on a γ-alumina characterized by a high-specific area (200 m^2/g) in order to obtain catalysts with properties indicated in Table 3. The catalysts precursors were then dried and subsequently calcined at 773 K under air.

2.1.3. Sulfided catalysts

Three different sulfidation methods have been carried out. The fresh CoMo and NiMo catalysts were presulfided under a 3 $l/h/g_{catalyst}$ H_2S/H_2 (15%, v/v) flow at 673 K during 120 min with a 5 K/min ramp and transferred to the XPS pre-chamber without any exposure to air. The obtained catalysts are also named Ni-0 and Co-0. The approximate value of chemical potential of sulfur corresponding to these sulfidation conditions (T and $p(H_2S)/p(H_2)$) is −0.87 eV. As explained by different authors [12,13,15,16], the chemical potential of sulfur is the variable representing the working sulfo-reductive conditions.

In the case of NiMo catalysts, the sulfidation was also undertaken under H_2S in N_2, and the other conditions were left unchanged as for Ni-0 and Co-0. The resulting sulfided catalyst is named Ni-2. The value of chemical potential of sulfur corresponding to the sulfidation with pure H_2S in absence of H_2 is close to −0.50 eV.

The fresh NiMo catalyst was also sulfided under model molecules in a continuous fixed-bed co-current upflow reactor. The feed, composed of cyclohexane (74.12%, w/w), toluene (20%, w/w) and dimethyldisulfide (5.88%, w/w), was fed into the reactor at a LHSV of 4 h^{-1} and a pressure of 6 MPa. Hydrogen was supplied with a ratio $H_2/HC = 450$ nl l^{-1}. Temperature was raised from 273 to 623 K with a 2 K/min

Table 2
Origin of different aged CoMoP/Al_2O_3 catalysts

Origin	Feedstocks	Processing time (days)	Catalyst	T (K)	$p(H_2S)/p(H_2)$	$\Delta\mu_S$[a]
Fresh	–	0	Co-0	–	–	–
Industrial plant	GO	730	Co-A	620–650	~0.1	−0.87
	GO	730	Co-B	620–650	~0.1	−0.87
	GO	730	Co-C	620–650	~0.1	−0.87
Pilot plant	SRGO	25	Co-D	608	~0.095	−0.85
	GO coker	34	Co-E	593–608	~0.043	−0.89
	HGO	15	Co-F	633–643	~0.008	−1.03

[a] $\Delta\mu_S$ is the chemical potential of sulfur (expressed in eV) and is used in Fig. 6 (the reader could refer to [12,13,15,16] for a detailed explanation of this thermodynamic variable representing the working conditions T and $p(H_2S)/p(H_2)$).

Table 3
Composition of fresh catalysts oxides

Catalysts	NiO (wt%)	CoO (wt%)	MoO_3 (wt%)	P_2O_5 (wt%)	Co(Ni)/Mo[a]
Ni-0/Ni-1/Ni-2	2.6	–	15	6	0.55
Ni-0.2	0.9	–	17	5.7	0.19
Ni-0.4	1.8	–	17	5.7	0.40
Ni-0.5	2.7	–	17	5.7	0.52
Co-0	–	4	18	4	0.50
Co-0.0	–	–	20.1	5.7	0.00
Co-0.1	–	0.9	19.3	5.7	0.11
Co-0.3	–	1.9	19.5	5.7	0.28
Co-0.4	–	2.8	18.4	5.7	0.43

[a] Atomic ratio determined precisely by XPS as the ratio between the absolute amount of promoter and the absolute amount of molybdenum.

ramp. A 1 h step was observed before cooling the reactor to 423 K. At this stage, all fluids were stopped. The catalyst was downloaded from the reactor and transferred to the XPS pre-chamber without any exposure to air. The catalyst obtained is named Ni-1. The approximate value of chemical potential of sulfur corresponding to these sulfidation conditions (T and $p(H_2S)/p(H_2)$) is −0.89 eV.

2.1.4. Reference oxidic catalysts

Reference catalysts were prepared in order to study the hydrogenating activity evolution as a function of the promotion rate without any significant coke deposit excepted the coke deposited during the activity measurement. Oxidic catalysts were prepared in the same way as for Ni-0 and Co-0. The quantities of nickel and cobalt present in the impregnation solution were changed while Mo loading was always the same in order to vary the Co(Ni)/Mo ratio of the catalyst. The metal compositions are summarized in Table 3. They are referenced as Ni(Co) *x.x*, where *x.x* is the atomic Ni(Co)/Mo ratio determined by XPS.

Resulting catalysts were sulfided under H_2/H_2S, in the absence of any hydrocarbon source, as for Ni-0 and Co-0. The ex situ method with a H_2S/H_2 gas mixture prevents the samples from coking during the sulfidation step. These sulfided catalysts were directly transferred to the XPS pre-chamber without any exposure to air. For the catalytic tests the catalysts were loaded on the oxidic catalyst form and sulfided with model molecules as described above. It was considered that the two sulfidation routes, in situ or ex situ, were similar.

2.2. Analytical method

The spent catalysts, as referenced in Tables 1 and 2, washed in toluene reflux and dried were analyzed without further treatment after air exposure. The pretreatment described in Section 2.1.1 did not lead to an extent of metal oxidation. Non-published works carried out in IFP showed that the coke formed inhibited the oxidation of MoS_2 particles. Fresh catalysts described in Table 3 were presulfided before analysis.

XPS measurements have been performed with an Axis Ultra-Kratos spectrometer using monochromatic Al Kα radiation ($h\nu$ = 1486.6 eV) and equipped with a hemi-spherical analyzer operating at fixed pass energy of 40 eV. The spot size on the sample was 700 μm × 300 μm. The recorded photoelectron binding energies were referenced against the C 1s contamination line at 284.6 eV. The XPS spectra of Mo 3d, Ni 2p, S 2p, Al 2p, P 2p, O 1s were recorded and analyzed using casaXPS software Version 2.0.71 after applying a Shirley background substraction and Gaussian (30%)–Lorentzian (70%) decomposition parameters.

A significant quantity of reference samples were analyzed previously to that work and used for the complex decomposition of the XPS spectra. Various sulfided and non-sulfided samples (containing only Mo or Ni or Co species) were analyzed to furnish the required data for the rigorous decomposition of the spectra. Each satellite peak is correlated to the binding energy, the intensity and the full width at half maximum (FHWM) of the main peak to which it is associated. An unsupported MoS_2 sample revealed two peaks at 228.8 eV (MoS_2 $3d_{5/2}$) and 231.9 eV (MoS_2 $3d_{3/2}$). The ratio between the two areas and FHWM and the two binding energies have been conserved for further decomposition. A MoO_3/Al_2O_3 sample was then analyzed and revealed two peaks at 233.0 eV (Mo^{6+} $3d_{5/2}$) and 236.1 eV (Mo^{6+} $3d_{3/2}$). As for MoS_2 species, the same parameters were linked together. Furthermore, a MoS_2/Al_2O_3 sample was analyzed and two Mo^{5+} contributions were added at 229.8 eV (Mo^{5+} $3d_{5/2}$) and 232.9 eV (Mo^{5+} $3d_{3/2}$). The same procedure was applied to nickel and cobalt elements analyzing successively $Ni(Co)^{2+}/Al_2O_3$, Ni(Co)-Sulf/Al_2O_3, and Ni(Co)MoS/Al_2O_3 samples. We should notice that the presence of molybdenum on the first oxidic sample does not modify the position of the $Ni(Co)^{2+}$ peaks. In the case of Ni(Co), some satellites are observed and are defined during the successive samples analysis.

The Mo 3d spectra (Fig. 1A) were curve-fitted [17] using six main components corresponding to the electron levels $3d_{5/2}$ and $3d_{3/2}$ in three oxidation states (Mo^{4+} and Mo^{6+}, respectively attributed to MoS_2 and Mo oxide environment while Mo^{5+} is identified as an intermediate state of oxisulfide type). S 2s contributions respectively attributed to sulfur and sulfate compounds were identified but not taken into account in the quantification. Ref. [17] explains in details this method in the case of CoMo catalysts. A similar methodology was used for the NiMo catalysts. The Co(Ni) 2p envelope was decomposed using three main contributions (Fig. 1B and C)

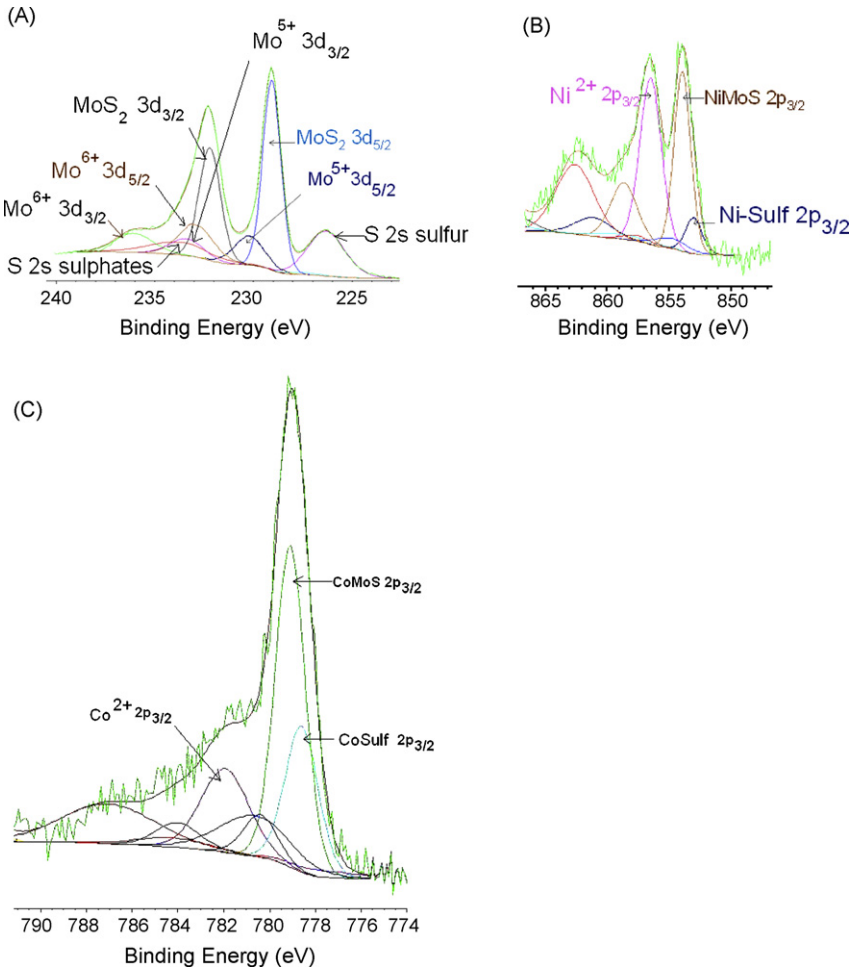

Fig. 1. XPS decomposition: (A) Mo 3d (Ni-E), (B) Ni $2p_{3/2}$ (Ni-E), and (C) Co $2p_{3/2}$ (Co-0).

corresponding to a sulfided phase named "Co(Ni)Sulf" (with binding energies at 778.1 and 853.1 eV, respectively for Co and Ni, respectively), an oxide contribution $Co(Ni)^{2+}$ representing Co(Ni) in interaction with alumina (at 781.4 and 856.1 eV), and the "Co(Ni)MoS" contribution described as the mixed phase (at 778.6 and 854.0 eV). For the sake of clarity, satellites have not been indicated Fig. 1B and C, even if they are well identified thanks to the energy difference and area relationships with the main peaks.

The S 2p spectra were curve-fitted as described in Ref. [17]. S-Sulf corresponds to sulfur atoms in MoS_2, or Ni-Sulf species and the sulfates correspond to sulfur atoms strongly oxidized. A supplementary contribution must be added in the decomposition of the S 2p signal. It is called SOx and corresponds to sulfur atoms partially oxidized. It could be compared to the Mo^{5+} amount previously obtained.

The XPS decomposition led to the quantification of the absolute amount of each species as follows:

$$[j] = \frac{A_j/S_j}{\sum_{i=1}^{i=n} A_i/S_i} \times 100 \quad (1)$$

where A_i is the measured area of the species i, S_i is the sensitivity factor of the atom related to the species i (furnished by the manufacturer) and $[j]$ is the absolute amount of the species j.

From the absolute amounts of the various species, we can calculate the promotion rate which is defined as the percentage of Co(Ni) atoms engaged into the mixed "Co(Ni)MoS" phase, relatively to the total amount of Co(Ni) in the freshly sulfided sample (2):

$$\mathrm{PR} = \frac{[\mathrm{Co(Ni)MoS}]}{[\mathrm{Co(Ni)}]_0} \times 100 \quad (2)$$

where 0 refers to the freshly sulfided sample.

We distinguish the promotion rate from the promoter ratio. The promoter ratio is defined as the Co(Ni)/Mo ratio in the slabs (3):

$$\left(\frac{\mathrm{Co(Ni)}}{\mathrm{Mo}}\right)_{\mathrm{slabs}} = \frac{[\mathrm{Co(Ni)MoS}]}{[\mathrm{MoS_2}]} \quad (3)$$

To perform TEM analysis, the powdered catalysts were dispersed in ethanol. Two droplets of the solution were deposited on a Cu grid and dried. The sample was covered by a thin layer of an epoxy resin to prevent charging during TEM analysis. Shortly after preparation, the sample was analyzed with a FEI Tecnai FEG microscope with a 200 kV electron

beam and equipped with an EDX energy dispersive spectrometer. MoS_2 morphology was studied by TEM imaging in the bright field mode. At least 15 micrographs (each corresponding to ca. 4000 nm^2) were evaluated for each sample. Semi-quantitative estimation of the MoS_2 features was carried out by observing ca. 350 particles for each catalyst. The promoter segregation was investigated by TEM–EDX detection under analytical probe (1.0 nm) conditions, leading to Co(Ni)/Mo ratio calculated for about 20 particles. Ni–K, Co–K, Mo–K lines were used for this analysis.

XRF analysis was also performed and provided information on the overall composition of each catalyst.

2.3. Activity measurements

The hydrogenation activity of the spent catalysts was determined on toluene hydrogenation, in a continuous fixed-bed reactor. Experiments were carried out at 623 K and 6 MPa over 30 cm^3 of catalysts. The feed and reaction products were analyzed by FID gas chromatography with an apolar CP-SIL 5CB column. The first order activity was expressed relatively to the molybdenum amount.

2.4. DFT calculations

We indicate firstly that most of the DFT results used in this paper are extracted from the companion paper by Krebs et al. published in this volume [12]. In addition, we carried out more specific calculations of anthracene adsorption on the M-edge of the NiMo active phase. Anthracene is considered as a possible precursor for coke formation. In this case, we use the stable chemical states of the M-edge of the NiMo nano-crystallite in working conditions as determined in Ref. [12]. The adsorption energies are expressed as follows:

$$E_{ads} = E(\text{edge} + \text{anthr.}) - E(\text{anthr.}) - E(\text{edge} + n\text{S}) - nE(\text{H}_2) + nE(\text{H}_2\text{S}) \quad (4)$$

where E(edge + anthr.) is the total energy of the edge with the adsorbed anthracene molecule, E(anthr.) is the total energy of the isolated anthracene molecule, E(edge + nS) is the total energy of the M-edge with the stable sulfur coverage (n) in working conditions and before anthracene adsorption, $E(H_2)$ and $E(H_2S)$ are the total energies of H_2 and H_2S involved in the removal of S atoms from the edge during anthracene adsorption.

We use the VASP software based on the GGA-PW91 exchange functional [18,19] and 3D-periodic boundary conditions. A (3,3,1) k-point mesh was used to discretize the Brillouin zone of the slab's cell containing one MoS_2 sheet with five metallic layers perpendicular to the edge orientation and four nonequivalent edge sites (Ni–Ni–Mo–Mo). This atomic structure of the M-edge of NiMo active phase is extracted from Ref. [12]. The electronic convergence criterion was fixed at 0.01 meV and the geometric convergence was reached when forces are smaller than 0.05 eV/Å.

3. Results

3.1. Catalysts deactivation

The deactivation has firstly been investigated by performing activity tests on various spent catalysts (described in Tables 1 and 2). The hydrogenation activity of spent catalysts has been measured by following the toluene conversion. Since the molybdenum amount is not exactly the same on each spent catalyst, activities have been normalized per weight of molybdenum of the fresh catalyst. The first order activities are respectively found to be 0.33 and 0.19 $h^{-1}\,g_{Mo}^{-1}$ on fresh NiMoP and CoMoP catalysts. As expected, we observe (Fig. 2A) that the toluene hydrogenation activity decreases while processing time increases on NiMoP catalysts. The activity seems to be rapidly affected, being divided by two on catalysts from pilot plant (Ni-E to Ni-G). This series of catalysts tends to represent an intermediary state of deactivation. Afterwards, the deactivation process slows down and the resulting activities reach 10–30% of the initial activity at the life-end. The same conclusion can be drawn for CoMoP catalysts (Fig. 2B) even if in that case the deactivation seems to be less significant. At the end of catalysts life, NiMoP and CoMoP have the same activity (0.06 $h^{-1}\,g_{Mo}^{-1}$). The following part presents the results of characterization carried out on the spent catalysts in order to explain these observed deactivations.

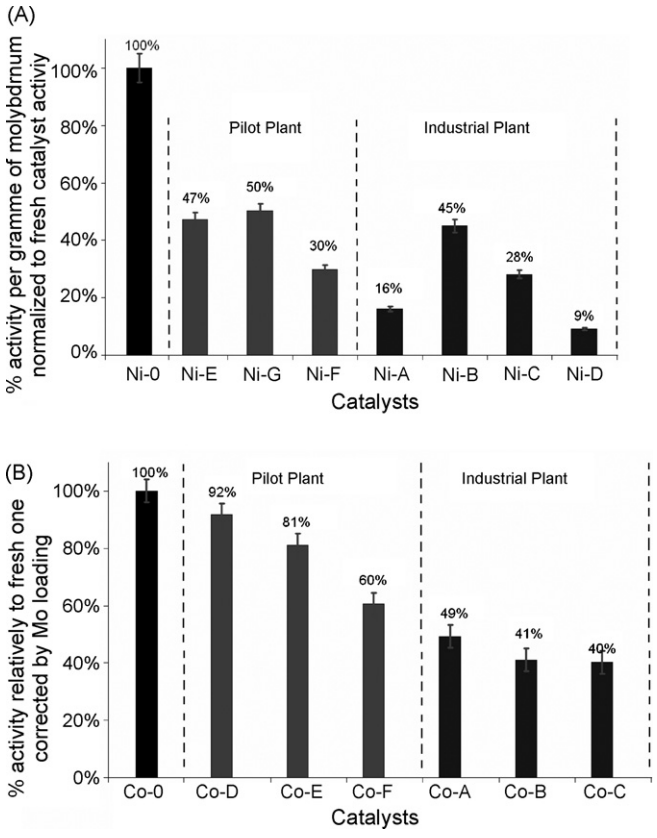

Fig. 2. Activities (toluene hydrogenation) of spent catalysts normalized with activity of fresh catalyst: (A) NiMoP catalysts and (B) CoMoP catalysts.

Table 4
Stacking and average sizes measured by TEM analysis

Origin	Catalyst name	Stacking	Size (nm)	Co(Ni)/Mo[a]		
				Average	Minimum	Maximum
Reference	Ni-0	1.9 ± 0.9	3.7 ± 1.4	0.23	0.17	0.29
Pilot plant	Ni-E	1.8 ± 0.9	3.6 ± 1.6		n.d.	
	Ni-G	1.8 ± 0.8	4.2 ± 1.9	0.12	0.05	0.18
Industrial plant	Ni-A	1.5 ± 0.7	3.7 ± 1.6	0.12	0.03	0.22
Reference	Co-0	2.5 ± 1.2	3.5 ± 1.7	0.20	0.12	0.29
Pilot plant	Co-D	1.6 ± 0.9	3.6 ± 1.5	0.20	0.09	0.48
Industrial plant	Co-A	1.8 ± 1.5	4.1 ± 2.1	0.10	0.06	0.24

[a] Ratio in MoS_2 particles by EDX measurements.

3.2. Changes of stacking and size during aging

We have characterized the evolution of stacking and size of catalysts particles occurring during catalysts life through TEM measurements. The results are presented in Table 4. Even on a completely deactivated catalysts (Ni-A), there is no effective modification of the MoS_2 crystallites morphology, which suggests that deactivation is not linked to MoS_2 sintering. Particles size varies between 3.7 and 4.2 nm for NiMoP catalysts and between 3.5 and 4.1 nm for CoMoP catalysts, which indicates that the stacking and size of MoS_2 sheets does not depend strongly on the promoter. Besides, for each catalyst, the stacking remains very low and almost unchanged.

An example of TEM images is presented in Fig. 3 for the Ni-A case (IP). Images are similar for all spent catalysts and we did not evidence the formation of Ni_3S_2-like or Co_9S_8-like crystallites of size greater than 1 nm (visible by TEM).

We have also coupled TEM observations with an EDX analyzer in order to evaluate the average chemical composition of the MoS_2 slabs. The average Ni/Mo or Co/Mo ratio taken from quantification on 15 MoS_2 slabs analysis is reported in Table 4. The Ni/Mo ratio decreases from 0.23 on Ni-0 to 0.12 on Ni-A and Ni-G, spent catalysts, while no variation of the ratio is observed by X-ray fluorescence analysis. The tendency is not so clear when MoS_2 slabs are decorated with cobalt. Indeed the Co/Mo ratio appears steady (0.20) between Co-0 and the one taken from pilot plant (Co-D). The decrease seems to appear for higher processing times reaching 0.10 on Co-A (IP). We might propose from EDX quantification and TEM observation that if the promoter segregates, it results to highly dispersed particles (beyond TEM resolution). Nevertheless we cannot totally exclude the formation of such small aggregates. Higher TEM resolution could have evidenced such formation.

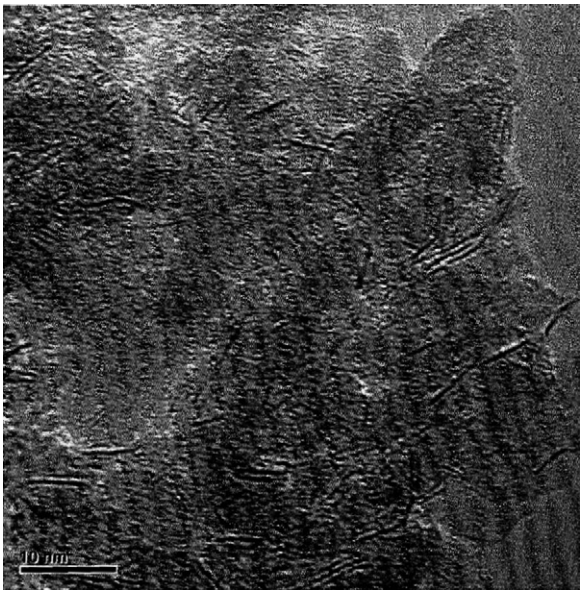

Fig. 3. TEM image on spent catalyst Ni-A (taken from industrial plant).

3.3. Evolution of the promotion rate (XPS)

For steady stacking and size features properties, it seems that the promoter amount in the MoS_2 crystallites decreases with processing time. We have intended to explore in more details this variation by performing XPS measurements. We have focused on the spectra of the metals participating to the active phase (Mo, Ni, Co). The evolution of the spectra are presented in Fig. 4.

Some preliminary observations can be drawn before any quantitative analysis of the spectra. In Fig. 4A and B presenting the evolution of molybdenum spectra, the main shape is characterized by the two peaks of MoS_2 $3d_{5/2}$ (ca. 229 eV) and $3d_{3/2}$ (ca. 232 eV). The structure remains consequently that of sulfided molybdenum. Nevertheless, the presence of a peak at ca. 236 eV (Mo^{6+} $3d_{3/2}$) indicates that some part of molybdenum is oxidized on spent catalysts (Ni-D, Ni-E and Co-B) exposed to the air after downloading the reactor. In agreement with XRF measurements we notice from the quantification of all surface elements (Table SM1) that the raw signal of molybdenum slightly decreases on the spent catalyst Ni-D (IP). The evolution of the Ni $2p_{3/2}$ spectra (Fig. 4C) is as expected. The shape of Ni 2p signal for both Ni-0 and Ni-2 fresh references samples are similar and mainly correspond to a sulfided Ni environment. However, high changes are observed on Ni-D and Ni-E spectra, samples coming respectively from industrial and pilot plant. The presence of a peak at ca. 856 eV attributed to Ni^{2+} state indicates that the oxidation rate of nickel is high on spent catalysts. It is also worth to notice that the raw signal of nickel highly decreases on the spent catalysts Ni-D and Ni-E

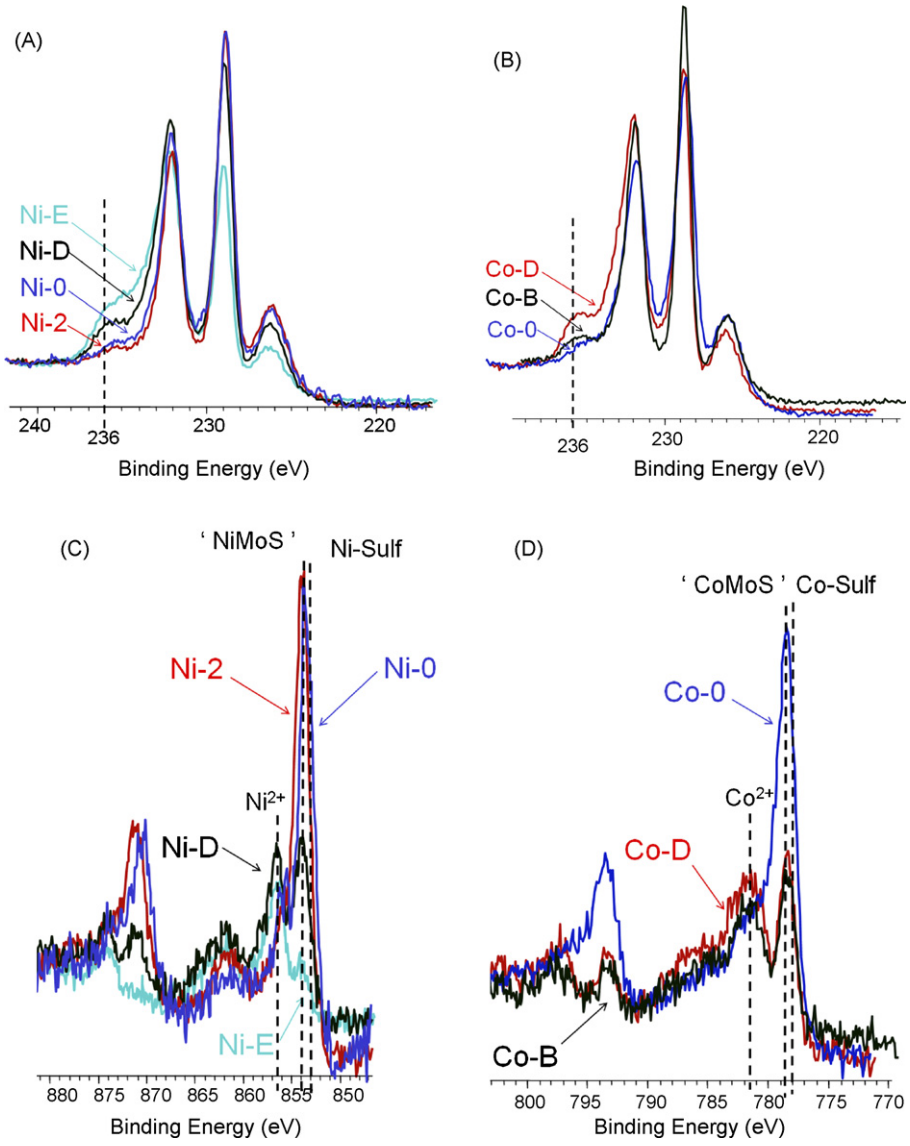

Fig. 4. XPS spectra comparison: (A) molybdenum of NiMoP/Al_2O_3 catalysts, (B) molybdenum of CoMoP/Al_2O_3 catalysts, (C) nickel on NiMoP/Al_2O_3 catalysts, and (D) cobalt on CoMoP/Al_2O_3 catalysts.

(Table SM1). The same observations can be drawn from the Co $2p_{3/2}$ spectra evolution (Fig. 4D). The spent catalyst Co-B from industrial plant also exhibits a lower promoter amount as determined by the quantification results (Table SM2) and an increase of the oxide contribution as shown with the higher contribution at 781.4 eV. The promoter spectra changes will be quantified and further discussed in more details.

We have firstly investigated the changes in the active phase composition of NiMoP/Al_2O_3 catalysts. Fig. 5A reports the amount of nickel for various fresh and spent catalysts and its repartition between ''Ni-Sulf'' (which could be Ni_2S_3, Ni_9S_8 or NiS), the nickel oxide (Ni^{2+}) and the nickel found in the mixed phase ''NiMoS''. These results show that the ''NiMoS'' proportion decreases when the catalyst deactivates. From this repartition a promotion rate has been defined by Eq. (2) where the reference sample is Ni-Sulf-0 (or Co-Sulf-0) in order to take into account the variation of the overall promoter amount. We can observe, from Table 5, that the promotion rate measured by XPS continually decreases with processing time. A similar behavior is observed for CoMoP catalysts (Table 6). The decrease of the mixed phase signal is accompanied by two other phenomena. The first one is an increase of the metals oxidation of the metals, as shown by the evolution in molybdenum species distribution. In Fig. 5B, the repartition between the three oxidation states (MoS_2, Mo^{6+} and Mo^{5+}) has been reported. We can see that Mo^{6+} and Mo^{5+} phases are slightly growing with processing time while the sulfided one (MoS_2) tends to decrease. We observed the sulfates formation (Table 5) which confirms the oxidation phenomenon. The oxidation is probably due to the reaction with air which occurs while unloading the catalyst from the reactor. It will affect nickel and molybdenum, but not necessarily in the same way. By quantifying molybdenum oxidized species (Mo^{5+} and Mo^{6+}) between fresh and spent catalyst, we can calculate the proportion of the ''NiMoS'' phase affected by oxidation. The results show that oxidation

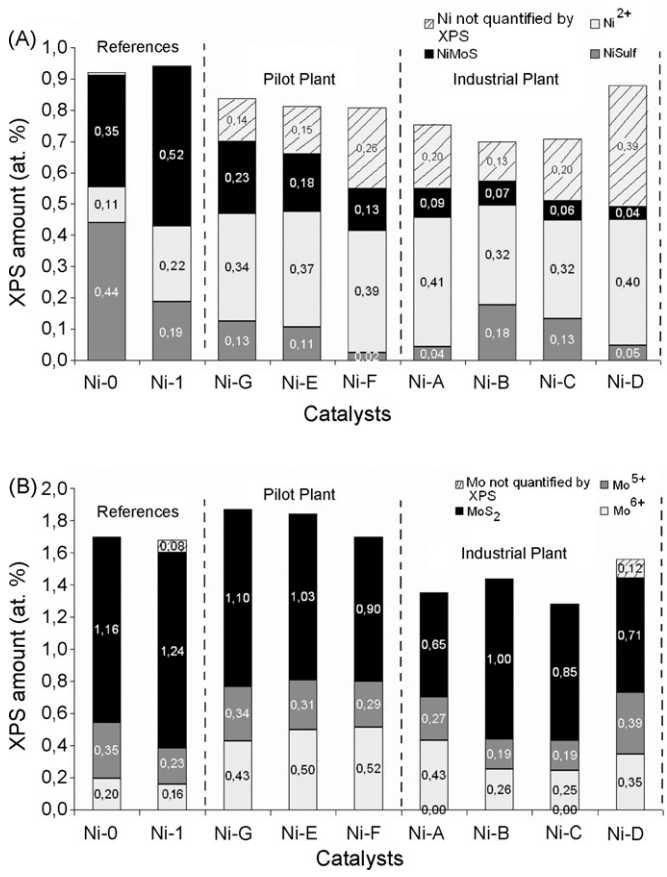

Fig. 5. XPS distribution of metals in freshly sulfided and spent NiMo catalysts: (A) nickel and (B) molybdenum (the values indicated in this graph correspond to the absolute amounts determined according to Eq. (1). The cumulated values of the three different oxidation states corresponds to the elements proportion indicated in Table SM1).

cannot be held responsible for the whole promotion rate decrease.

The second phenomenon revealed by Fig. 5A is the loss of a significant part of nickel which is not quantified on the various spent catalysts. Indeed only 55% of the initial nickel (48% of the initial cobalt) quantified on the fresh catalysts by XPS remains at the end of lifetime, while no significant change was observed on the nickel amount measured by X-ray fluorescence analysis. The nickel amount on spent catalysts evaluated by XPS has been corrected with the X-ray fluorescence nickel content in order to estimate the part of the nickel not quantified by XPS. The reason of the loss of the Ni signal will be further discussed.

The initial ''CoMoS'' phase proportion on fresh catalyst appears to be lower than the ''NiMoS'' phase. They are respectively found at 40% (Co-0) and 66% (Ni-2) of promoter in the fresh mixed phase. This difference tends to be attenuated in working state. Ni-E to Ni-G promotion rates (15–25%) are closed to Co-D, Co-E and Co-F promotion rates (20–23%). At life-end the promotion rate is lower on NiMoP type catalysts (4–10%) than it is on the CoMoP type (10%).

3.4. Relation between toluene hydrogenation activity and XPS promotion rate

Relative hydrogenation activities have been plotted against relative promotion rate in Fig. 6A (NiMoP) and in B (CoMoP). The reference fresh promoted catalysts described in Table 3 have been added on the graphs in order to represent the influence of Ni/Mo and Co/Mo ratio without coke effect. The hydrogenation activity of the NiMoP catalysts is correlated to the promotion rate (Eq. (2)) determined by XPS except for Ni-C which presents a different behavior. Silicon contaminant might be responsible for the higher observed activity than the one predicted by the promotion rate evolution for Ni-C. In the case of CoMoP catalysts, the activity is linearly related to the promotion rate for all spent catalysts.

4. Discussion

These results firstly reveal that the decrease of the XPS signature of the promoter in the mixed phase is the main phenomenon observed during the deactivation process. Two main reasons may explain this decrease:

Table 5
Promotion rate (PR) and metals' repartitions by XPS over spent and freshly sulfided $NiMoP/Al_2O_3$ catalysts

Origin	Catalysts name	PR (Ni)[a] (%)	$(Ni/Mo)_{slabs}$[b]	Mo repartition (at.%)			Ni repartition (at.%)			S repartition (at.%)		
				MoS_2	Mo^{5+}	Mo^{6+}	Ni-Sulf	Ni^{2+}	NiMoS	S-Sulf	SO_x	Sulfates
Reference	Ni-0	39	0.30	68	21	11	48	12	40	91	9	0
	Ni-1	57	0.42	76	14	10	20	24	56	93	7	0
	Ni-2	66	0.46	78	13	9	18	16	66	78	22	0
IP	Ni-A	10	0.14	48	20	32	7	76	17	56	11	33
	Ni-B	8	0.07	69	13	18	32	56	12	76	3	21
	Ni-C	7	0.07	66	15	19	25	63	12	68	4	28
	Ni-D	4	0.06	49	27	24	10	82	8	51	4	45
PP	Ni-E	20	0.18	56	17	27	17	56	27	62	9	29
	Ni-F	15	0.15	53	17	30	4	72	24	58	10	32
	Ni-G	25	0.21	59	18	23	18	49	33	61	9	30

[a] Promotion rate calculated according to Eq. (2) with Ni-Sulf-0 as a reference (the nickel amount are found to be similar on the various references as shown in Table SM1).

[b] Ni/Mo ratio in the MoS_2 slabs calculated from XPS results (Eq. (3)).

Table 6
Promotion rate (PR) and metals' repartitions by XPS over spent and freshly sulfided $CoMoP/Al_2O_3$ catalysts

Origin	Catalyst name	PR (Co)[a] (%)	$(Ni/Mo)_{slabs}$[b]	Mo repartition (at.%)			Co repartition (at.%)			S repartition (at.%)		
				MoS_2	Mo^{5+}	Mo^{6+}	Co-Sulf	Co^{2+}	CoMoS	S-Sulf	SO_x	Sulfates
Reference	Co-0	40	0.32	63	23	14	29	31	40	81	19	0
IP	Co-A	10	0.11	65	15	20	27	51	22	80	3	17
	Co-B	10	0.09	72	11	17	19	62	19	85	2	13
PP	Co-D	23	0.23	51	17	32	4	66	30	65	9	26
	Co-E	22	0.22	51	18	31	5	68	27	63	8	29
	Co-F	20	0.22	48	14	38	4	71	25	57	8	35

[a] Promotion rate calculated according to Eq. (2) with Co-Sulf-0 as a reference sample.
[b] Co/Mo ratio in the MoS_2 slabs calculated from XPS results (Eq. (3)).

- Part of the promoter atoms may have segregated in the carrier or inside the coke and cannot be quantified by XPS.
- The coke deposit at the edges of the Co(Ni)MoS crystallite which masks the promoter signal. In this case, the distance crossed by the emitted photoelectrons from Co(Ni) in order to reach the surface may become so large that only a small fraction can escape without any scattering event taking place. This phenomenon is also evidenced by the increase in the carbon amount quantified by XPS.

It must be added that TEM observations of NiMoS particles coupled with EDX analyses showed that the Ni/Mo ratio decreases with time-on-stream from 0.23 (Ni-0) to 0.13 (Ni-A). With this technique, only the largest crystallites are characterized which explains why the initial ratio is lower than the one found by means of XPS (0.33 on Ni-0). Nevertheless, since coke cannot mask the EDX signal, the decrease of the ratio from 0.23 to 0.13, evidences that some NiMoS particles (at least the largest) are affected by the Ni segregation.

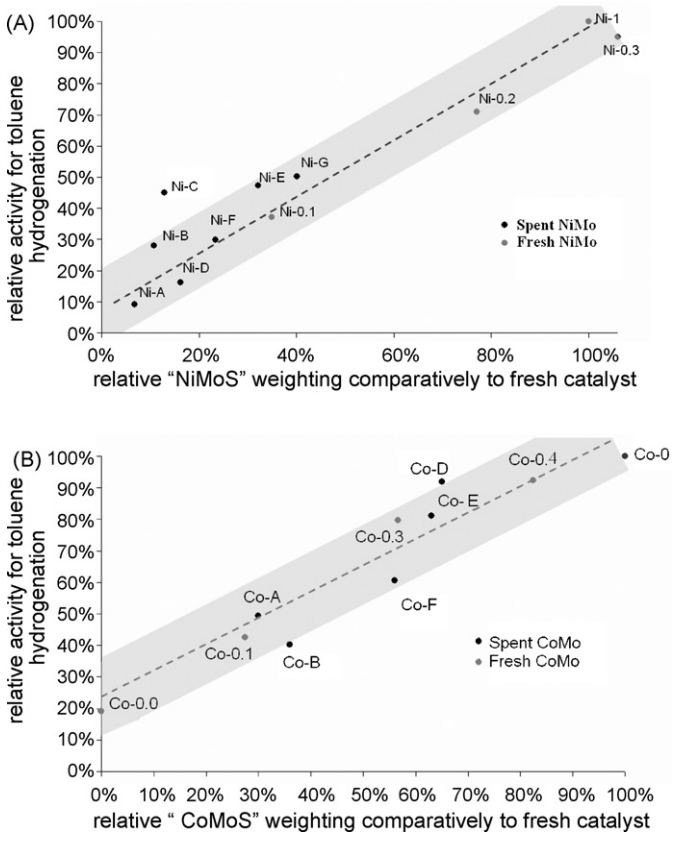

Fig. 6. Evolution of hydrogenation activity (relatively to fresh catalyst ones per gram of molybdenum) with promotion rate (Eq. (2)) measured by XPS (normalized to fresh catalysts ones): (A) NiMoP catalysts and (B) CoMoP catalysts.

To propose an interpretation of this phenomenon, we can first refer to the experimental studies by Breysse et al. [9,10] based on Mössbauer spectroscopy of aged CoMoS catalysts which have also revealed the loss of the mixed phase in reductive conditions. We will now consider the DFT results by Krebs et al. reported in this issue [12] on the stability of NiMoS and CoMoS phases in HDT conditions. According to this work, the 2D-morphology of Co(Ni)MoS crystallites (i.e. proportion of M-edge/S-edge) and the stability of the promoter at the edges of the crystallites is given in Fig. 7 as a function of the chemical potential of sulfur, $\Delta\mu_S$ representing the working conditions. The phase diagrams for the Co(Ni)MoS active phases reveal the reaction conditions where partial and total segregation of the promoter from the mixed phase may occur. First, we observe that nickel is stabilized on the M-edge for $\Delta\mu_S$ higher than −1.3 eV and on S-edge for potential higher than −1.05 eV. For cobalt, the behavior is different since it is stabilized on M-edge for potential higher than −0.9 eV and on S-edge for potential higher than −1.05 eV. According to the catalysts sulfidation conditions indicated in Section 2.1, the chemical potential of sulfur during sulfidation of Co-0 and Ni-0 is about −0.87 eV, while it is around −0.50 eV for Ni-2 and −0.89 for Ni-1. Taking into account these values, the positions of the fresh catalysts are indicated by the full circles (Ni-0, Ni-2, Co-0) and the dashed circle (Ni-1) on the diagrams of Fig. 7. The morphology and the promoter edge content of the nanocrystallite can thus be deduced. In Fig. 8 the Gibbs–Curie–Wulff equilibrium morphologies and edge atomic structures are represented on the basis of the proportion of M-edge given by Fig. 7. The average crystallite size determined by TEM is also chosen for this representation. For Ni-2 (N_2/H_2S sulfidation), the S-edge and M-edge of crystallites are fully decorated by the promoter leading to the morphology of Fig. 8A with a high Ni/Mo ratio of 0.40 closed to the promoter ratio (Eq. (3)) found by XPS (0.42–0.46). In contrast, in more reductive conditions as used for sulfiding Ni-0, and Co-0 (H_2/H_2S sulfidation) the edge

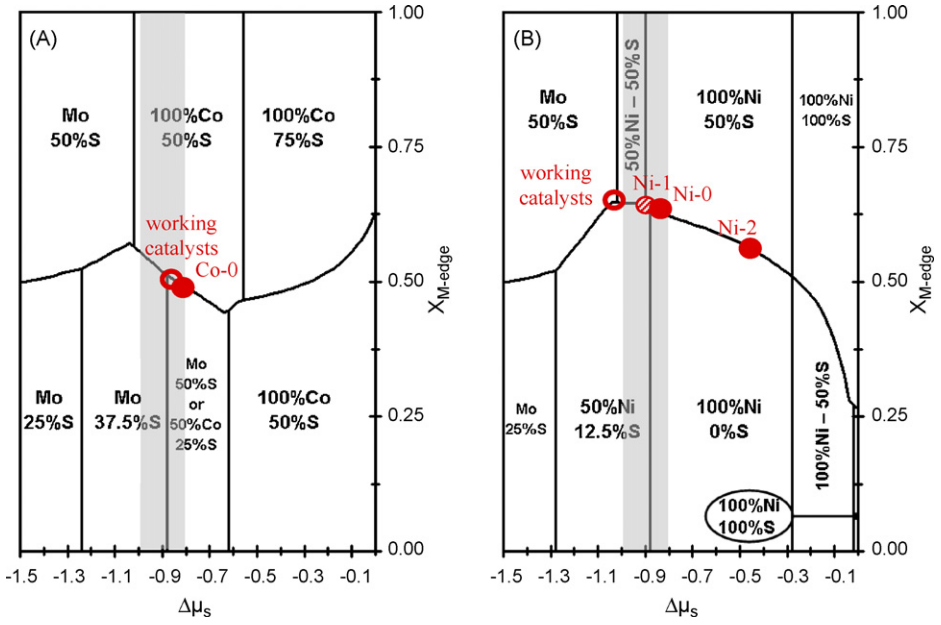

Fig. 7. Morphology diagrams (extracted from [12]) for the nano-crystallites: (A) CoMoS and (B) NiMoS. The proportion of M-edge (in ordinate) is indicated by the black broken line. The S-edge compositions are reported above the black line and the M-edge compositions are below this line. For $X_{\text{M-edge}} = 1$ (resp. 0), the shape is a perfect M-edge (resp. S-edge) triangle. For $X_{\text{M-edge}} = 0.5$, the shape is a perfect hexagon. According to the sulfo-reductive conditions, the positions of the fresh (Ni-0, Ni-1, Ni-2) are given by the full and dashed circles and of the working catalysts (in industrial plant) by empty circles.

promoter content is decreased either at the M-edge or at the S-edge or at both edges. Fig. 8B and C may be relevant models of the crystallite's morphology for the NiMoS and CoMoS. The Ni/Mo ratio in the slabs reported in the legend of Fig. 8 are also consistent with the XPS characterization. In particular, the ratio is initially 1.4 times higher with nickel (Ni-2) than with cobalt (Co-0) (Tables 5 and 6). If we now focus on the NiMo catalyst (Ni-1) sulfided with dimethyldisulfide at a partial pressure of H_2S of 0.05 and $T = 623$ K, the value of the chemical potential of sulfur is −0.9 eV, which leads to a Ni/Mo ratio of 0.42 as revealed by XPS. This means that the initial state of the NiMo particles is closed to the dashed circle reported in Fig. 7B and the corresponding morphologies and promoter content represented in Fig. 8A. This second type of freshly sulfided catalyst is thus close to the frontier between four possible domains of NiMo particles (Fig. 7B) which explains that, at this value of the chemical potential of sulfur, it is possible to reach a Ni/Mo ratio beyond 0,40. We also note that this ratio is closer to the one found for the Ni-2 catalyst and higher to the one found on Co-0.

For the various working conditions of NiMoS in industrial or pilot plants reported in Table 1, the chemical potential of sulfur, $\Delta\mu_S$, varies between −1.01 and −0.95 eV [14]. For these values, the empty circle reported on the diagrams of Fig. 7A indicates that the stability of the promoter at the edge is questioned. For the NiMoS catalysts, part of the promoter atoms may thus segregate either from M-edge or from the S-edge during the reaction. The Gibbs–Curie–Wulff equilibrium morphologies are reported in Fig. 8C and the corresponding promoter ratio is about 0.17. This value is close to the XPS ratio (0.15–0.21) found for the spent catalysts from pilot plant (Ni-E, Ni-F, Ni-G) and higher than for catalysts taken from industrial plant, 0.06–0.14 (Ni-A to Ni-D). This suggests that for catalysts used in industrial plants, the processing time and specific environment conditions imposed by the petroleum feeds may lead to a supplementary loss of the Ni promoter content from the S- and M-edges.

For the CoMoS catalysts, in the stable state found in the reaction conditions, the Gibbs–Curie–Wulff equilibrium morphology is very close to the fresh catalyst (Fig. 8B) and the corresponding Co/Mo ratio should remain about 0.29. Such values are slightly higher than the XPS analysis about 0.22 (Table 6) for the spent catalysts from pilot plant (Co-D, Co-E, Co-F). As for the NiMoS active phase, the CoMoS phase used in industrial plant (Co-A, Co-B) exhibits a lower Co/Mo ratio (0.09–0.11), revealing that a second phenomenon may occur in industrial plant leading to a supplementary loss of the XPS signal of the mixed phase.

To identify the reason for the supplementary loss of NiMoS active phase in industrial plant, we notice that the reaction conditions imply that the catalyst stable state is closed to the domain where Ni has fully segregated from the S-edge (Fig. 7A). As a first consequence, slight variations may occur around this chemical potential of sulfur and may shift the stable state in a region where the Ni–Mo mixed sites are lost from the S-edge. In addition, coke precursors may also play a role in the segregation of the promoter from the M-edge. Using the density functional theory (DFT) as described in Section 2.4, we have calculated the adsorption energy of coke precursors such as anthracene molecule on the M-edge of a partially substituted NiMoS. The stable M-edge structure for NiMoS catalysts (with Ni–Ni–Mo–Mo configuration determined in [12]) in the reaction conditions of industrial plant and pilot plant is the one reported in Fig. 8C. The adsorption configuration reported in Fig. 9A shows that the π mode of interaction involving two

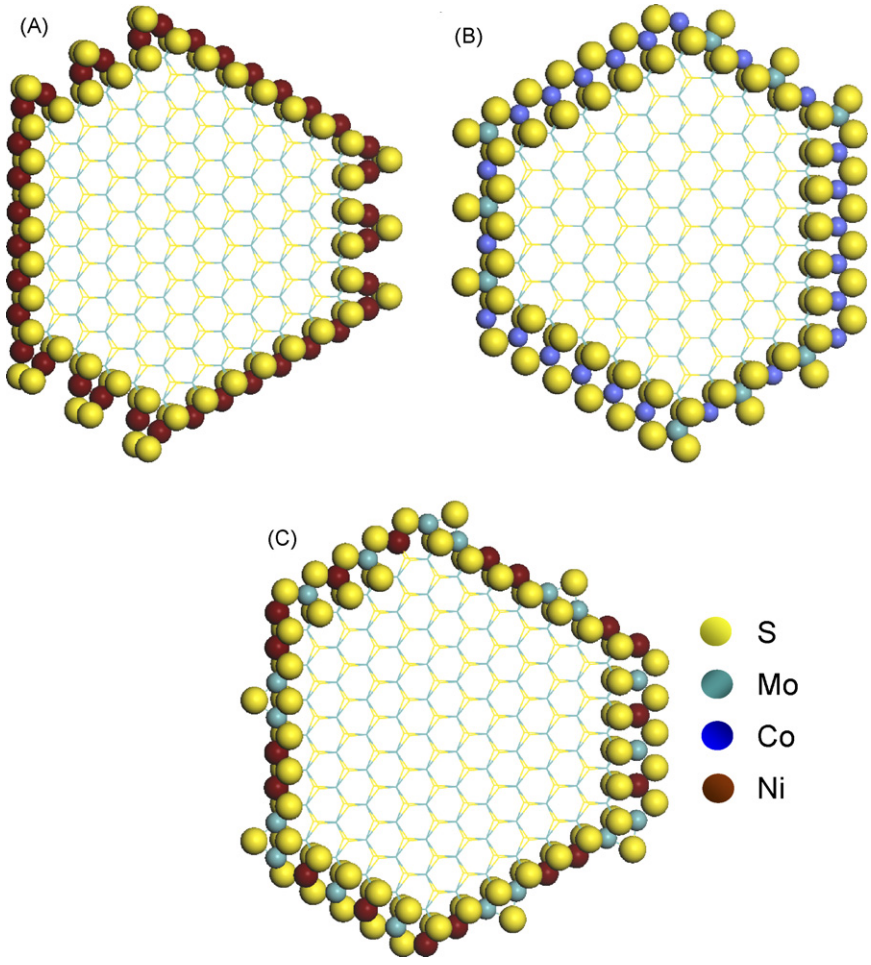

Fig. 8. DFT models of the promoted MoS_2 nano-crystallites consistent with XPS analysis coupled with TEM measurements—(A) fresh NiMoS catalyst (Ni-2) with Ni/Mo = 0.40: fully substituted by Ni on both edges, (B) working CoMoS catalysts with Co/Mo = 0.29: M-edge partially substituted by Co, (C) working NiMoS catalyst (Ni/Mo = 0.17): both edges are partially substituted by Ni.

phenyl rings on top of two neighbouring Mo sites is strongly favored on this edge. For the M-edge with no S-atom (assuming $n = 0$ in Eq. (4)), the corresponding adsorption energy is −306 kJ/mol. However, before anthracene adsorption, the M-edge promoted by Ni is covered by one sulfur atom according to [12]. This S-atom must be removed from its bridging position between the two Mo-atoms (Fig. 8C) also involved in the interaction with anthracene. The resulting energy balance (given by Eq. (4) with $n = 1$) is found to be close to athermal, which means that in heavy feeds to be treated and containing coke precursors, the M-edge of the NiMoS particle may be poisoned by coke precursors (as represented in Fig. 9B). After a large processing time, the coke growth at the M-edge would strongly poison this edge leading to the possible supplementary decrease of the XPS signal observed for most aged NiMoS catalysts from industrial plant. In a subsequent step, we cannot

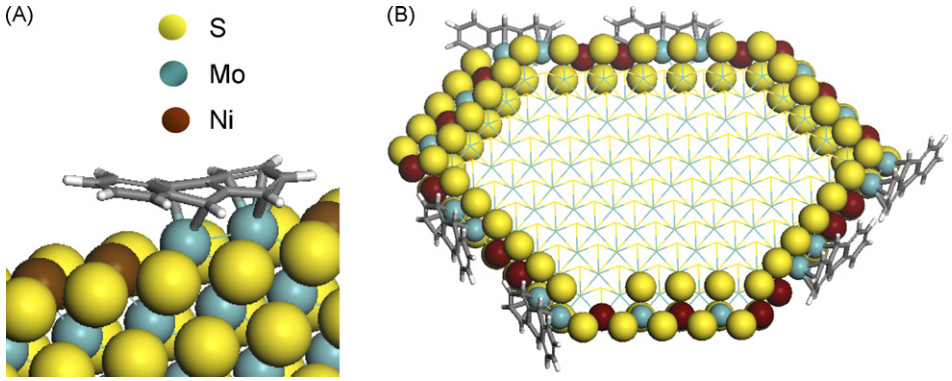

Fig. 9. Ab initio simulation of coke precursor adsorption (anthracene) on the Ni–Mo mixed sites of the M-edge: (A) optimized configuration of anthracene in the periodic cell used for the DFT calculation and (B) aged NiMoS particles poisoned by anthracene molecules.

exclude that the promoter may be also extracted from the edges as a consequence of the coke precursor adsorption to form two distinct phases: non-promoted MoS_2 crystallites and segregated promoter atoms trapped inside coke deposit (not visible anymore by XPS). Again, the decrease in activity due to the poisoning of the mixed Ni–Mo sites or to their complete loss will be dramatic as observed in toluene hydrogenation test (Fig. 6A).

In the case of CoMoS catalysts, the reaction conditions in industrial plant ensure a slightly higher chemical potential value (−0.87 eV). According to the work by Krebs et al. [12], the stable state of the CoMoS morphology is represented in Fig. 8B involving the presence of mixed Co–Mo sites. However, in a coking environment and after a long processing time, the mixed sites located at the M-edge are also suspected to be lost, following a similar process as previously proposed for NiMoS catalysts. Hence, the promoter ratio in the Co-A and Co-B catalysts (lower than 0.16 according to XPS) may be due to a similar adsorption mechanism of coke precursors as previously described for NiMoS catalysts.

5. Conclusion

The present study investigated the stability of ''NiMoS'' and ''CoMoS'' phases in working state combining XPS, TEM, EDX, catalytic tests and DFT simulations. We found out that promoter segregation is at the origin of the modifications on recorded XPS spectra. These results led to a deactivation scheme in which the evolution of the promotion rate monitors the hydrogenating activity. XPS results show that the oxidation phenomenon cannot be held responsible for the total lowering of the promotion rate and most of the decrease is due to the proportion of nickel which is not quantified. At this stage, we suggest that the loss of the promoter signal observed by XPS is attributed to two phenomena.

On the one hand, DFT calculations show that part of Ni and Co may be destabilized from the edges of the NiMoS and CoMoS crystallites due to the reaction conditions (high temperature and highly reductive environment). XPS and EDX show that Ni may segregate and the use of DFT calculations suggests that the nickel segregation occurs from both M- and S-edges of the crystallite, whereas Co may only segregate from the M-edge. This result highlights the different behaviors between CoMoS and NiMoS catalysts in HDT reaction conditions.

On the other hand, it has been suggested that coke formation in industrial plant occurring after a long processing time and after coke precursors (such as anthracene) adsorption on the M-edge of NiMoS may also be at the origin of a supplementary segregation mechanism or the poisoning of the crystallites M-edge. This may explain the very low Ni/Mo or Co/Mo observed by XPS in spent catalysts from industrial plant after several processing days. We thus propose that the coke deposit could capture a great part of the promoter, leading to the loss of mixed Ni–Mo and Co–Mo sites which are critical for the HDT activity, as illustrated in the paper by Gandubert et al. published in this volume [20].

Acknowledgements

Authors gratefully acknowledge P. Lecour for XPS measurements, L. Sorbier, A.L. Taleb and F. Moreau for TEM/EDX analysis and A. Gandubert for supplying fresh CoMo catalysts with variables Co/Mo.

Appendix A. Supplementary data

Supplementary data associated with this article can be found, in the online version, at doi:10.1016/j.cattod.2007.09.007.

References

[1] S. Kasztelan, H. Toulhoat, J. Grimblot, J.P. Bonnelle, Appl. Catal. 13 (1984) 127.
[2] H. Topsøe, B.S. Clausen, F.E. Massoth, Hydrotreating Catalysis, Springer, Berlin, 1996, p. 29.
[3] M.A. Callejas, M.T. Martinez, T. Blasco, E. Sastre, Appl. Catal. A 218 (2005) 181.
[4] S.K. Sahoo, S.S. Ray, I.D. Singh, Appl. Catal. A 278 (2004) 83.
[5] J.G. Weissman, S. Lu, B.M. Mc.Elrath, J.C. Edwards, Deactivation of hydrotreating catalysts, in: Proceedings of the 12th Canadian Symposium on Catalysis, Banff, Alberta, Canada, May 25–28, 1992.
[6] L.P.A.F. Elst, S. Eijsbouts, A.D. Van Langeveld, J.A. Moulijn, J. Catal. (2000) 95.
[7] F. Pedraza, S. Fuentes, M. Vrinat, M. Lacroix, Catal. Lett. 62 (2007) 121.
[8] B.M. Vogelaar, P. Steiner, T.F. Van Der Zijden, A.D. Van Langeveld, S. Eijsbouts, J.A. Moulijn, Appl. Catal. A: Gen. 318 (2007) 28.
[9] M. Breysse, R. Frety, B. Benaïchouba, P. Bussière, Radiochem. Radioanal. Lett. 59 (1983) 265.
[10] M. Breysse, R. Frety, M. Vrinat, P. Grange, M. Genet, Appl. Catal. 12 (2) (1984) 165.
[11] S. Eijsbouts, L.C.A. Van Den Oetelaar, R.R. Van Puijenbroek, J. Catal. 229 (2005) 352.
[12] E. Krebs, B. Silvi, P. Raybaud, Catal. Today 130 (2007) 149.
[13] P. Raybaud, J. Hafner, G. Kresse, S. Kasztelan, H. Toulhoat, J. Catal. 189 (2000) 129.
[14] P. Raybaud, Appl. Catal. A: Gen. 322 (2007) 76.
[15] H. Schweiger, P. Raybaud, H. Toulhoat, J. Catal. 212 (2002) 33.
[16] C. Arrouvel, M. Breysse, H. Toulhat, P. Raybaud, J. Catal. 232 (2005) 161.
[17] A. Gandubert, C. Legens, D. Guillaume, S. Rebours, E. Payen, Oil Gas Sci. Technol. – Rev. IFP 62 (1) (2007) 78.
[18] G. Kresse, J. Furthmüller, Phys. Rev. B 54 (16) (1996) 11169.
[19] G. Kresse, J. Furthmüller, Comput. Mater. Sci. 6 (1996) 15.
[20] A. Gandubert, E. Krebs, C. Legens, D. Guillaume, P. Raybaud, Catal. Today 130 (2007) 149.